Available online at www.sciencedirect.com
SCIENCE DIRECT
Biochimica et Biophysica Acta 1758 (2006) 730–737
BIOCHIMICA ET BIOPHYSICA ACTA
BBA
http://www.elsevier.com/locate/bba

Brownian dynamics investigation into the conductance state of the MscS channel crystal structure

Taira Vora [a], Ben Corry [b], Shin-Ho Chung [a,*]

[a] Department of Theoretical Physics, Research School of Physical Sciences, The Australian National University, Canberra, A.C.T. 0200, Australia
[b] School of Biomedical, Biomolecular and Chemical Sciences, The University of Western Australia, Crawley, WA 6009, Australia

Received 16 December 2005; received in revised form 23 March 2006; accepted 5 April 2006
Available online 26 April 2006

Abstract

We suggest that the crystal structure of the mechanosensitive channel of small conductance is in a minimally conductive state rather than being fully activated. Performing Brownian dynamics simulations on the crystal structure show that no ions pass through it. When simulations are conducted on just the transmembrane domain (excluding the cytoplasmic residues 128 to 280) ions are seen to pass through the channel, but the conductance of ~ 30 pS is well below experimentally measured values. The mutation L109S that replaces a pore lining hydrophobic residue with a polar one is found to have little effect on the conductance of the channel. Widening the hydrophobic region of the pore by 2.5 Å however, increases the channel conductance to over 200 pS suggesting that only a minimal conformational change is required to gate the pore.

Keywords: MscS; Ion channel; Mechanosensation; Brownian dynamic; Electrostatic; Conductance

1. Introduction

Mechanosensitive ion channels provide the means by which cells respond to a range of mechanical stimuli including molecular agitation and osmotic pressure, and underlie the senses of touch and hearing. The mechanosensitive channel of small conductance (MscS) is a stretch activated channel found in *Escherichia coli* that responds to forces within the inner membrane to alleviate osmotic shock [1–4]. They are also voltage dependent [3,5] and show a slight anion selectivity (P_{Cl}/P_{Na} ~ 1.5–3.0) [4,6].

Recently, a crystal structure of the MscS channel was determined to 3.9 Å resolution, which showed the channel to be a homoheptamer with each subunit containing 3 transmembrane domains [7]. One of these domains (TM3) lines the pore while the other two (TM1 and TM2) contact the membrane where it is posited they would respond to bilayer tension. Furthermore, these outer helices were postulated to also act as the voltage sensors of the channel, as each helix contains an arginine residue near the middle of the membrane. A large cytoplasmic domain was also present, containing a central chamber connected to the bulk solution by a series of wide openings that may be responsible for ion selectivity [1].

Initially, the imaged structure of the channel was posited to be in an open, conductive state [7]. The narrowest portion of the transmembrane region of the pore was claimed to have a diameter close to 10 Å, easily wide enough to pass ions. However, since the determination of this structure there has been much discussion regarding this point. Bezanilla and Perozo [8] noted that if this structure indeed represented the channel in an open state, then envisaging how it could be closed while still maintaining 7-fold symmetry was difficult, and suggested that other regions of the protein, such as the TM2–TM3 loop could form part of the gate. Cysteine crosslinking experiments suggest that the closed state of the channel is significantly different from the imaged conformation [9].

Two molecular dynamics simulations cast further doubts on the conductance state of the imaged channel. One found that water was unlikely to pass through the narrowest region of the pore and that there was a huge barrier to ion conduction, and thus claimed that the imaged structure of the channel was not in its open state [10]. A second series of simulations also found that the density of water in the pore oscillated about a low value. However, they also discovered that removal of constraints

* Corresponding author.
E-mail address: shin-ho.chung@anu.edu.au (S.-H. Chung).

0005-2736/$ - see front matter © 2006 Elsevier B.V. All rights reserved.
doi:10.1016/j.bbamem.2006.04.014

holding the protein near the imaged structure led to a narrowing of the pore to a hypothesised closed state [11].

Determining the state of the imaged structure of the protein is important for understanding the mechanism of gating within this class of pore [12]. If the structure represents the channel in the open state, then gating obviously involves a closure of the pore by the TM3 or nearby regions. Alternatively if the channel is closed in this configuration, then this implies that ion conduction is not prevented by a physical blockage, but rather by other means. There are a number of ways by which the behaviour of water in the pore can block ion conduction. Green et al. [13–15] suggested that water could accumulate in high density or be immobilised by the surface geometry or large electric fields, and this could prevent ion conduction by creating a narrower effective pore through which ions could not pass with their hydration shell intact. These studies highlighted the role of charged or ionisable residues in fixing or releasing water. More recently a reverse gating process more applicable to the MscS channel has been proposed, as it has been found that narrow pores surrounded by non-polar residues can block ion conduction by providing an unfavourable home to water. If the water is at a low density in the pore, then again the ion will have to be stripped of its hydration shell to pass through the channel and thus there is a desolvation barrier rather than a physical blockage that can prevent ion conduction [16]. This 'hydrophobic gating' concept has been demonstrated in model pores [17,18] and is also believed by many to be at play in the acetylcholine receptor pore [19–23]. A small change in the radius or surface polarity of the region can be enough to open the pore. Indeed, Anishkin and Sukharev [10] conclude that such a hydrophobic gating mechanism underlies the function of the MscS channel. This suggestion gains credence from the observation that the replacement of central pore lining non-polar residues with polar ones increases the activity of the channel [24,25]. A final alternative is that the imaged structure of the channel neither represents the open nor the closed state of the channel, but an intermediate of the two, or a non-physical state induced by the process of crystallization.

In this paper we aim to investigate the crystal structure of the channel using Brownian dynamics simulations in order to determine the likely conductance of the channel. This mesoscopic technique allows for simulations to be run long enough to relate the channel current to the protein structure while still retaining some atomisitic detail, a task that is difficult with other methods. We also examine channel models in which the cytoplasmic domain has been removed, or the pore widened to help understand the functioning of MscS.

2. Methods

2.1. Channel models

2.1.1. Crystal structure

The MscS channel model is created using the crystal structure coordinates (1MXM) submitted by Bass et al. [7] to the Protein Data Bank. We locate the boundary separating the protein and the water-filled pore by tracing around van der Waals radius of the pore lining atoms. A three-dimensional, cylindrically symmetric pore, connecting the inside and the outside of the cell is created by determining the minimum radius of the pore for each z value and rotating this by 360°. The resulting radius is illustrated in Fig. 1A along with the atoms forming the protein and again in Fig. 2A. Bass et al. [7] claim that the pore has a minimum diameter near the residues L105 and L109 of nearly 11 Å. Our pore, however, has a diameter nearly half of this value. To examine whether this difference was caused by asserting axial symmetry, we also calculate the pore radius using the program HOLE [26] that does not make the assumption of axial symmetry. A comparison of the two pores is given in Fig. 2A. The radius of our symmetric pore, and that found using HOLE agree well throughout the narrow section of the pore, although the minimum pore radius found using HOLE at 3.1 Å is slightly larger than in the symmetric pore at 2.5 Å.

The narrow transmembrane region opens into a wider cytoplasmic chamber with a radius of over 25 Å before narrowing again at the intracellular end. The channel has a total charge of + 28e with an important charged R88 residue found on the TM2 pointing into the pore. This charge, located at $\sim z$=48 Å, plays a crucial role for ions entering the channel and is discussed in further detail in Section 3. In our simulations, the protein atoms are treated as point charges placed in their exact positions as found in the crystal structure.

2.1.2. Modified structures

The large cytoplasmic vestibule produces an obstacle in our Brownian dynamics (BD) simulations, as our program is currently unable to cope with a protein with extra-membrane regions surrounded by water as described in more detail below. For this reason, we perform simulations both including this region, and excluding it (as noted by the box in Fig. 2A, and discussed in Section 3).

To remove the cytoplasmic vestibule, we deleted the residues numbered from 128 through to 280. Notably, the total charge of the protein was not affected by this and remained at its original value of +28e. In this truncated structure, only the transmembrane pore region was used to create a three-dimensional boundary whose radius is illustrated in Fig. 2B. Once the intracellular residues were removed, the channel was centred about the z-axis. The residue R88, which was previously at

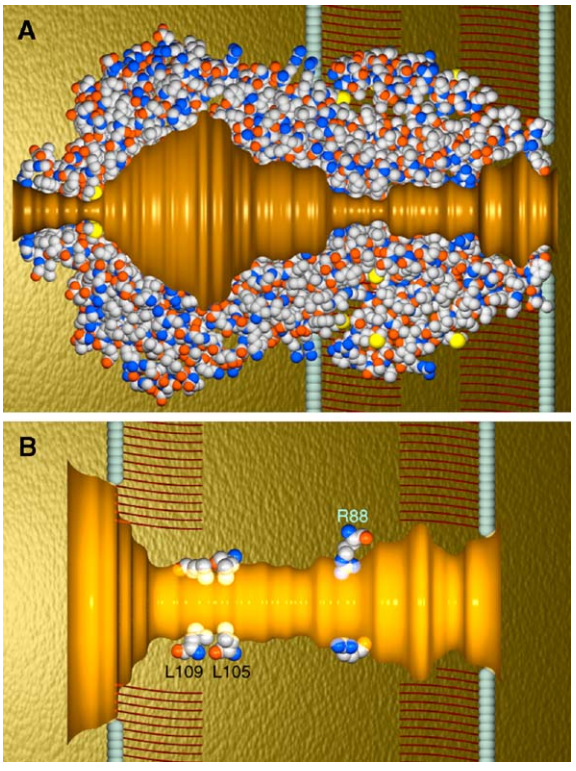

Fig. 1. MscS channel structures. (A) Schematic of the MscS crystal structure with the top half removed to reveal the pore. (B) Schematic of the transmembrane region of the *expanded structure*. The highlighted residues, starting from the intracellular side, are residues L109 and L105 that line the expanded part of the channel, and R88, the only charged amino-acid residue lining the pore.

z=48 Å, after centering now lay at z=12 Å. This structure will be referred to as the *truncated crystal structure* for the remaining sections of this article.

We have also performed simulations on the L109S mutant structure known to increase channel activity [25] and studied using molecular dynamics by Anishkin and Sukharev [10]. Replacing the hydrophobic pore-lining leucine residue with the more hydrophilic serine was shown to aid the entry of water into this region of the pore. The channel radius is almost unchanged by this mutation as shown by the dashed line in Fig. 2C. Here again, the cytoplasmic vestibule was removed and simulations were conducted only on the transmembrane portion of the protein. We will refer to this structure as the *L109S mutant*.

Finally, to investigate the effect of widening the pore, we created a structure with an expanded pore using CHARMM. The cytoplasmic region (residues 128–280) that was later to be removed in the Brownian dynamics simulations was fixed in the imaged position. A weak harmonic constraint of 1 kcal/mol/Å was applied to all atoms of the transmembrane region to hold it in position overall, while allowing pore-lining atoms to move. We applied a radially outward force relative to the z-axis with a force constant of 50 kcal/mol/Å decreasing to zero at r=8 Å to residues 80–120 that form the narrow part of the channel. Initially, 100 steps of energy minimisation were performed using the steepest descent method. Then, in order to reduce stresses within the system, the constraints were reset to the new atom positions, and the system's energy was minimised for a further 100 steps. After this the cytoplasmic domain was removed, the channel was re-aligned and centred along the z-axis and a pore boundary was traced for use in Brownian dynamics simulations, as illustrated in Fig. 2B. The final structure has a minimum radius of 5 Å. This channel shape will be referred to as the *expanded structure*.

2.2. Simulation details

Once the channel models were created, we conducted Brownian dynamics simulations to determine the likely current that would pass through each structure. To do this, we attached reservoirs filled with K and Cl ions on either side to mimic the intracellular and extracellular solutions. The height of the reservoirs was controlled to provide the appropriate concentrations. The ions are initially assigned random positions and velocities and their motion is simulated using the Langevin equation,

$$m_i \frac{d\mathbf{v}_i}{dt} = -m_i\gamma_i\mathbf{v}_i + \mathbf{F}_R(t) + q_i\mathbf{E}_i + \mathbf{F}_S. \quad (1)$$

The first term on the right, $-m_i\gamma_i\mathbf{v}_i$, describes the frictional force experienced by an ion as it attempts to move through a fluid with a frictional coefficient of

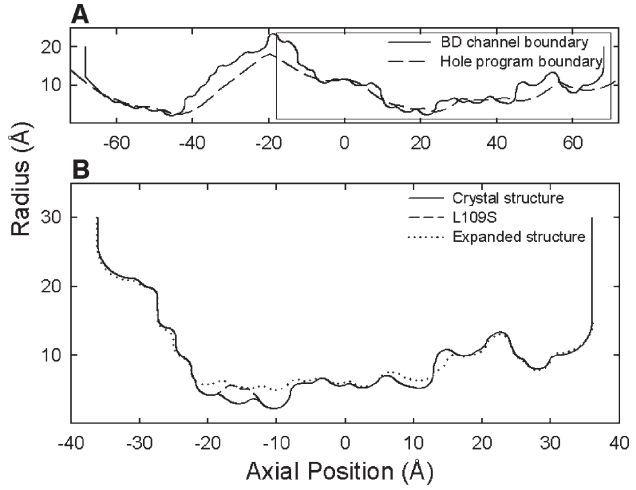

Fig. 2. MscS channel models. (A) The crystal structure boundary produced by the HOLE program (dashed line) plotted with the MscS channel boundary generated for the process of Brownian dynamics (solid line). This has been generated from the crystal structure coordinates. (B) The section in (A) selected by the box has been enlarged and centred about the z-axis. These are the truncated structures used for BD simulations. The transmembrane parts of the crystal structure (solid line), the L109S mutant boundary (dashed line), and the expanded boundary (dotted line) are shown here.

Table 1
Physical properties of ion types used in Brownian dynamics simulations

	K^+	Cl^-
Mass (kg)	6.5×10^{-26}	5.9×10^{-26}
Bulk diffusion ($m^2\ s^{-1}$)	1.96×10^{-9}	2.03×10^{-9}
Ionic radii (Å)	1.33	1.81

$m_i\gamma_i$. The second term, $\mathbf{F}_R$, is a random force arising from collisions of the ions with water molecules that are not treated explicitly in our simulations. Performing simulations on individual ions and water molecules requires large amounts of computational time, therefore we simplify the situation by treating the water molecules as a continuous dielectric medium. The second last term, $q_i\mathbf{E}_i$, describes the electrical force and is described below. Finally, the last term, $\mathbf{F}_S$, is a short-range force term that includes short range ion–ion and ion–protein interactions [27].

The electric force acting on an ion includes the effect of the applied potential, Coulomb forces between ion–ion pairs and ions and fixed charges in the protein, and the image forces the ions encounter as they approach the protein–water interface. These are computed by solving Poisson's equation:

$$\varepsilon_0 \nabla[\varepsilon(\mathbf{r})\nabla\phi(\mathbf{r})] = -\rho(\mathbf{r}) \quad (2)$$

in which $\varepsilon(\mathbf{r})$, $\phi(\mathbf{r})$ and $\rho(\mathbf{r})$ are the space dependent dielectric constant, electric potential and charge density respectively. The equation is solved using the boundary element method in which the boundary separating two dielectric media is divided into a number of sectors. The surface charge density on each sector induced by the charge on ions or on other sectors is calculated using an iterative approach. This method was tested extensively by Hoyles et al. [28,29] and others against the analytical solution for a point charge in a prolate spheroid boundary, as well as a simple model for a biconical channel and has been compared to the results achieved using a finite difference approach. We have also tested the accuracy of boundary element solution in our calculation of the electrostatic energy profiles by varying the number of boundary sectors used within the channel pore, more details of which are provided in Section 3.1. To avoid solving Poisson's equation at every step of the Brownian dynamics simulations, solutions for a number of 0, 1 and 2 ion configurations are stored in a set of lookup tables [30]. During the simulations values for the given ion configuration can be constructed from values interpolated from the tables. Dielectric constants of ε_p=2 and ε_w=60 are assigned to the channel protein and water filled regions respectively, and a Born energy barrier is introduced at the entrance and exit of the channel. This Born energy represents the energy barrier seen by an incoming ion as it enters from a region of water-filled higher dielectric to narrow pore with a lower dielectric. Although the membrane and protein core is known to have a low dielectric constant, its value in the aqueous environment inside the pore is less clear. It is likely that in the narrow regions of the channel water molecules are less able to orient to an electric field than in bulk solution. As it is not known what value is best to use, we use a value of ε_w=60 was found to yield the best agreement with experimental currents in previous simulations of the KcsA channel [33].

The Langevin equation is solved using an algorithm devised by van Gunsteren et al. [31,32]. The velocities are calculated every 100 fs with a shorter timestep of 2 fs inside the channel. Most of the forces are precalculated and stored in lookup tables which can be accessed when needed during the simulation [33]. A concentration of 100 mM KCl was used in the reservoirs for all BD runs with 55 pairs of ions in each reservoir. Further properties of the ions are given in Table 1. The current for each data point on the current–voltage curve was calculated by counting the number of ions that crossed the channel in a 7.2 μs simulation. For further information on the Brownian dynamics method we refer the reader to [27,33,34].

3. Results

3.1. Energy profiles

Electrostatic energy profiles were created by passing a single Cl ion through the channel at 1 Å intervals and solving Poisson's

equation to obtain its energy landscape inside the pore with no applied potential. When creating a multi-ion energy profile, one ion is placed in its equilibrium position in the channel and a second ion is brought in along the z axis from the outside. The internal ion is allowed to move to its minimum energy position within the channel, while the external ion is only allowed to equilibrate in the *xy* plane. The potential energy of the external ion is calculated at 1 Å steps. In order to test the validity of the boundary element solution, we varied the number of boundary sectors and solved Poisson's equation to calculate the potential energy seen by ions entering the channel. We tried 18,000 and 25,000 sectors spanning the protein water boundary. The results are found to be almost identical, with the maximum deviation of potential at a point along the *z*-axis between the two different sector counts being 4.25%.

3.1.1. Crystal structure

A Cl ion entering from the extracellular side sees a large energy well of over 300 kT attracting it into the centre of the transmembrane region, as shown in Fig. 3A. The bottom of the energy well lies at the location of the pore-forming R88 residue, around $z=48$ Å. Beyond this region, the narrowing of the pore, and the absence of charged residues near the protein–pore boundary inhibits the ion from traversing any further. The ion now sees a barrier of over 400 kT to move out of the energy well towards the intracellular side. This energy barrier terminates at residue ASP274 ($\sim z=-42$ Å), followed by a shallow energy well of 100 kT and finally another energy barrier to get out of the intracellular vestibule of the channel. The large energy barrier in the cytoplasmic chamber may be due to an approximation in the simulation. As noted above, we assign a low dielectric constant to all the space with radii greater than the pore boundary, including the protein and water that is likely to surround this region and do not account for the water filled portals in the side of the chamber. If this region was surrounded by water, the image forces can be expected to be weaker, that might make the cytoplasmic chamber a more favourable home for ions.

3.1.2. Modified structures

The truncated protein structure presents a similar energy profile to ions entering the extracellular end of the channel as shown in Fig. 3B. However, the ion sees a slightly smaller energy well of about 270 kT attracting it into the centre of the channel, again around the position of R88. Beyond this point, similar to that in the crystal structure, it sees an energy barrier of a similar magnitude that it must climb to reach the cytoplasmic end of the pore.

We will see later that ions have difficulty passing through the channel due to this energy profile. Ions are seen to conduct through the channel but the conduction is slowed by the narrowing of the pore around residue L109. We found that when the outer regions of the channel are filled with 8 Cl ions (this is the number of ions occupying this region at equilibrium, see Section 3.2) and a ninth ion is moved from $z=0$ to $z=-25$ Å (the narrow section of the channel), and its potential energy calculated, the ion sees an energy barrier of nearly 10 kT, making the passage through this region the rate limiting step for conduction. A further discussion of this has been provided in Section 3.2, where we study the average number of ions and their most likely positions within the various channel models.

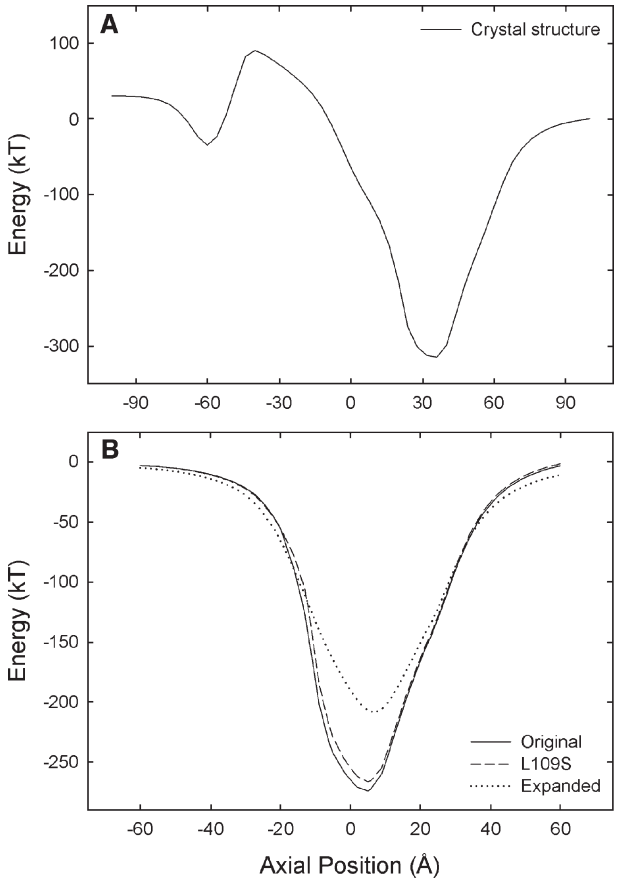

Fig. 3. Potential energy profiles of a single chloride ion are calculated at an applied potential of 0 mV. Poisson's equation is solved as the permeating ion is moved by 1 Å steps along the channel axis and its potential energy calculated. Profiles are shown for the crystal structure (A) and for the truncated crystal structure (solid line), L109S mutant (dashed line) and expanded (dotted line) structures (B).

The energy profile in the L109S mutant is very similar to that found in the truncated structure. This leads us to suspect that there would not be a drastic difference in the current found to pass through each channel.

On the other hand, a Cl ion entering the expanded channel sees quite a different energy landscape, also shown in Fig. 3B. As one would expect, the widening of the channel reduces the image forces on the ion, but also causes the attractive forces between the ion and the partial charges on the protein to weaken. This leads to the energy well in the centre of the channel to become shallower with a depth of 200 kT. We will see later from the Brownian dynamics results that this shallower well actually aids conduction. The permeating Cl ion no longer see an energy barrier of 10 kT when crossing the narrow region of the channel. In fact, it sees almost no barrier at all.

3.2. BD simulations

Next we performed Brownian dynamics simulations on all four channel structures to determine the current passing through

them. We tested the crystal structure with and without the intracellular domain, with the two different sets of boundary sectors used to calculate the electrostatic forces on ions (see Section 3.1) and found that the difference in the current–voltage curve results were within estimated errors.

3.2.1. Crystal structure

Brownian dynamics simulations were performed on the crystal structure of the MscS channel using a diffusion coefficient of 0.5 between $-3<z<10$ Å, 0.1 between $10<z<25$ Å and 0.5 between $25<z<60$ Å respectively, depending on the width of the pore, as suggested by molecular dynamics studies of narrow channels [35]. Ions were assigned their bulk diffusion coefficient in the cytoplasmic vestibule owing to its large volume.

The channel is expected to have a conductance of ~1 nS [3,36], but we found no ions permeating the crystal structure of channel in 5 μs of simulation each for 9 different applied potentials, ranging between ±150 mV. A plot of the average number of ions in the channel during the simulations is shown in Fig. 4. We find a total of 12 Cl ions in the channel at any given time. There are 10-Cl ions in the transmembrane region with 2 ions at the very end of the cytoplasmic region. The number of ions in the channel is quite high, but despite this no ions were able to cross the channel. We see a large number of ions sitting towards the extracellular side of the channel with two distinct peaks around the region of R88. Almost no ions are resident in the narrow region of the channel between residues L105 and L109, around $z=20$ Å. The histogram shows that the region between $z=0$ Å and $z=-55$ Å, consisting of the cytoplasmic vestibule is empty with no ions present at all. This leads us to believe that the central barrier across the cytoplasmic vestibule region seen in Fig. 3A is too high, hindering the movement of ions across this region. Once inside the transmembrane region, the ions are unable to move into the cytoplasmic chamber. Of course, our simulations assign a dielectric constant of $\varepsilon_p=2$ to all regions of the channel protein

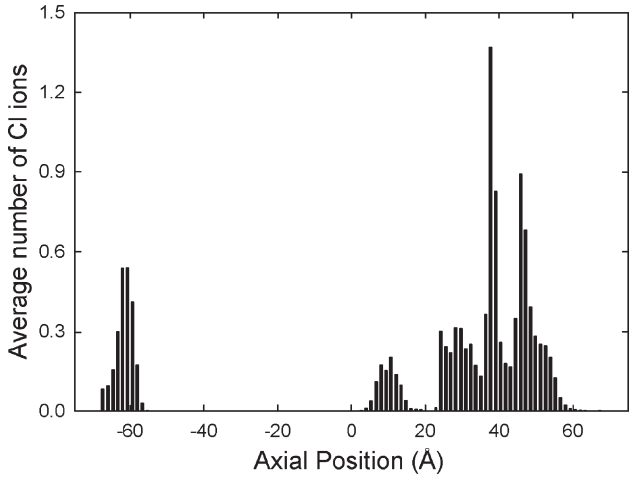

Fig. 4. Average number of chloride ions in the crystal structure at an applied potential of 0 mV. There are two distinct peaks corresponding to the position of the well in Fig. 3A. No ions are seen to occupy the cytoplasmic chamber. A total of 12 Cl ions are found to reside in the channel.

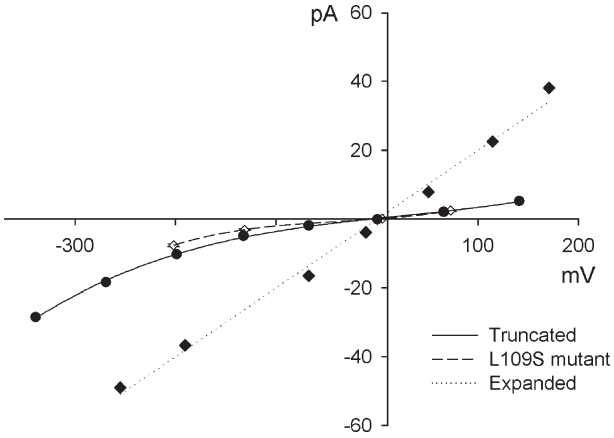

Fig. 5. Current–voltage relationships for the truncated structures. Solid line—crystal structure, dashed line—L109S mutant, dotted line—expanded structure. All simulations were carried out with symmetric solutions of 100 mM KCl and 55 pairs of ions in each reservoir. Each data point was calculated over a 7.2 μs simulation.

and we are currently unable to accurately model the cytoplasmic region that is surrounded by water. Is this limitation of the simulations the reason why we see zero current? A further discussion of the assumptions used in our methods to model Brownian dynamics and how it might affect the channel current is provided in the discussion below.

3.2.2. Modified structures

The current–voltage relationships for the three modified structures in which the cytoplasmic vestibule have been removed are plotted in Fig. 5. Diffusion coefficients of 0.4, 0.15 and 0.7 times the bulk value for chloride were used between $(-20<z<-8$ Å), $(-8<z<12$ Å) and $(12<z<30$ Å), respectively [35].

Unlike the crystal structure, ions do pass through the truncated structure during Brownian dynamics simulations. However, the current was found to be only 3.6±0.2 pA at ± 100 mV, much lower than the value of around 100 pA observed experimentally [3,36]. The channel is found to be selective, allowing only Cl ions to pass. The current–voltage curve is roughly linear at lower applied voltages but starts to show some non-linearity at below −150 mV.

The L109S mutant shows a slightly more asymmetric current of −3.8±0.3 pA at −100 mV and 2.24±0.3 pA at 100 mV. It is difficult, however, to determine whether this is a consequence of the mutation or a stochastic difference between simulations. At low currents the passage of one ion can cause a large variation in the current.

Once the pore was expanded the current was seen to increase dramatically, shown by the dotted line in Fig. 5. The current through the channel rose to 19.4±0.5 pA at +100 mV and −23.4±0.5 pA at −100 mV. This can be attributed to the lowering of the image repulsion from the channel walls around residue L109.

A histogram of the average number of Cl ions in the channel for the truncated crystal and L109S mutated structures is given in Fig. 6A. They both have a very similar distribution of ions in the channel. The plot is only slightly different to that seen for the crystal structure in Fig. 4, and both channels still contain 10 Cl

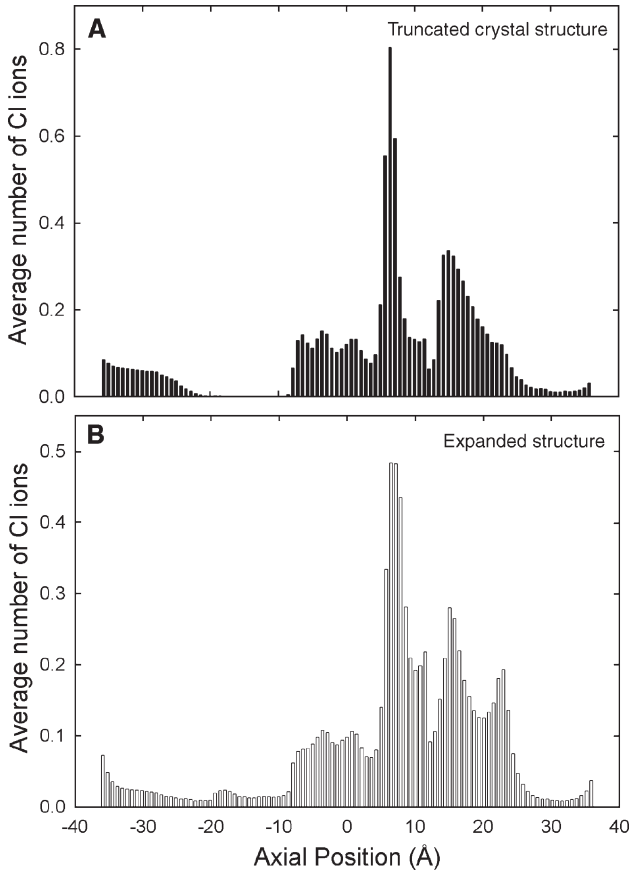

Fig. 6. A histogram of the average number of chloride ions in the channel. (A) Truncated crystal structure, (B) Expanded channel.

ions on average in the transmembrane section. The peaks in ion density are somewhat different to that found in the crystal structure. In this case ions are no longer tightly bound in the channel, but are seen to dynamically permeate through the channel, albeit at a slow rate which undoubtedly affects the time they spend in various 'binding sites' within the channel. Notably, ions rarely dwell in the narrow part of the channel between $-10<z<-20$ Å.

In the expanded channel, ions are seen to dwell throughout the channel, including the region between residues L105 to L109 as shown in Fig. 6B. This also corresponds to a large increase in the conductance of the channel. Together, these results imply that crossing this region of the channel was the rate limiting step for conduction in the narrower structures. Increasing the radius of this region of the channel means that ions experience a much lower repulsive image force from the non-polar residues that surround this part of the pore. Fewer ions (8.4) inhabit this channel than the narrower versions, a consequence of the higher throughput and smaller energy well shown in Fig. 3B.

4. Discussion

Experimental studies have shown the MscS channel to have a conductance of ~1 nS at symmetric concentrations of 100 mM KCl [3]. In our simulations, we failed to see any ions permeating through the recently crystallized structure of the channel [7].

This lack of current could be a consequence of limitations of our simulation scheme. Our method for conducting Brownian dynamics simulations and electrostatics calculations are designed for a protein without significant extracellular domains or side entrances to the pore. The current limitations of our approach mean that the seven cytoplasmic portals with radii of ~7 Å had to be closed off and treated as protein and the water surrounding the cytoplasmic domain cannot be modeled appropriately. We understand that this not only blocks possible entry points for ions into the chamber, but also increases the effective image forces experienced by ions once inside the chamber. The cytoplasmic chamber undoubtedly plays an interesting role in the conduction process and it would be preferable to model it accurately. Indeed, it has been postulated that this region could be responsible for sorting through ions of opposite valencies [1]. In an initial attempt to investigate the role of the cytoplasmic chamber, we rotated the protein so that the z-axis now passed through two of the cytoplasmic portals creating a continuous pore. We conducted BD simulations by attaching reservoirs on either side of the portals and no applied potential to study the significance of this intracellular chamber. We found that after 1.6 μs of simulation, there were approximately 2 K ions and 3 Cl ions inside the chamber, roughly the same ratio as the measured permeability of the channel. It is thus plausible that this intracellular region of the protein is responsible for discriminating between ion species.

However, to avoid the limitations of our methodology and to clarify the state and function of the transmembrane region, we performed simulations with the cytoplasmic domain removed. It was hoped that doing this might clarify the reason why the ions were not crossing the channel. Removing this region increased the conductance of our model, suggesting that the simplified treatment of the extramembrane region may have been influencing our results. However, we found that ions passed at only a low rate and that the narrow, hydrophobic region of the pore was hindering conduction.

Molecular dynamics simulations have shown that the L109S mutant increases the likelihood of forming a continuous chain of water through the pore by creating a more hydrophilic environment in the center of the channel [10]. It is hypothesised that such a mutation should also aid the passage of ions. In our Brownian dynamics simulations this mutation has little effect. This is not entirely surprising, and most likely reflects the way that water is treated within these simulations. In our simulations, water is treated as a continuous dielectric medium that exudes a random force on ions inside the channel. We have assigned a dielectric constant of 60 throughout the pore to represent the presence of water, and therefore, as far as our simulations were concerned, there were water molecules present around the L109 region even before the mutation was made. In our case, the mutation is only changing the partial charges near the pore, not its water content. In our simulations, ions find it difficult to cross this narrow section of the pore regardless of whether it is lined by polar or non-polar residues.

Widening the channel, on the other hand, has an acute effect on the channel current. Increasing the channel diameter near the hydrophobic residues L105 and L109 region by only ~2.5 Å

caused an 8-fold increase in the current. This enormous increase in current suggests that only minimal conformational changes would be required to open or close the channel. It should be stressed that our expansion of the pore was not designed to replicate the open state of the channel. Rather, it was used to help elucidate the conductance state of the imaged structure of the protein and to investigate qualitatively the size of structural rearrangement that is required to open the pore.

The MscS channel has been shown to have only a slight preference for anions over cations with both species able to permeate through the channel [3]. In our simulations, no cations were seen to cross the channel. As the crystal structure of the channel is in a non-conductive state in our simulations, it cannot tell us the whole story about ion permeation. If the conformation of the protein is different in its conducting state, then these may make the pore more attractive to cations [1]. Alternatively, some of the positively charged residues may become deprotonated in physiological conditions, or cations may be chaperoned through the channel by anions.

5. Conclusion

The fact that ions find it difficult to pass through either the entire crystal structure or transmembrane domain of the channel during Brownian dynamics simulations suggests that the protein may not have been crystallized in its open state. The rate limiting step in conduction is for ions to pass the narrow hydrophobic region of the pore near residues L105 and L109. We find that by replacing the pore-lining hydrophobic residue L109 with a polar serine does not increase the current through the channel. However, widening this section of the pore increases the conductance of the channel dramatically. A 2.5 Å radius increase has such a dramatic effect on the channel current suggesting that only minimal structural rearrangements may be required for channel gating.

Acknowledgments

This work was supported by grants from the Australian Research Council and the National Health and Medical Research Council of Australia. Calculations were performed on the Linux Cluster LC, the Alpha server SC and the SGI Altix cluster at the APAC National Facility.

References

[1] M.D. Edwards, I.R. Booth, S. Miller, Gating the bacterial mechanosensitive channels: MscS a new paradigm? Curr. Opin. Microbiol. 7 (2004) 163–167.
[2] B. Martinac, Mechanosensitive ion channels: molecules of mechanotransduction, J. Cell Sci. 117 (2004) 2449–2460.
[3] B. Martinac, M. Buechner, A.H. Delcour, J. Adler, C. Kung, Pressure-sensitive ion channel in *Escherichia coli*, Proc. Natl. Acad. Sci. U. S. A. 84 (1987) 2297–2301.
[4] S. Sukharev, Purification of the small mechanosensitive channel of *Escherichia coli* (MscS): the subunit structure, conduction and gating characteristics in liposomes, Biophys. J. 83 (2002) 290–298.
[5] C. Cui, D.O. Smith, J. Adler, Characterization of mechanosensitive channels in *Escherichia coli* cytoplasmic membranes by whole-cell patch clamp recording, J. Membr. Biol. 144 (1995) 31–42.
[6] A. Kloda, B. Martinac, Mechanosensitive channels of bacteria and archaea share a common ancestral origin, Eur. Biophys. J. 31 (2002) 14–25.
[7] R.B. Bass, P. Strop, M. Barclay, D.C. Rees, Crystal structure of *Escherichia coli* mscs, a voltage-modulated and mechanosensitive channel, Science 298 (2002) 1582–1587.
[8] F. Bezanilla, E. Perozo, Force and voltage sensors in one structure, Science 298 (2002) 1562–1563.
[9] S. Miller, M.D. Edwards, C. Ozdemir, I.R. Booth, The closed structure of the mscs mechanosensitive channel—Cross linking of single cycteine mutants, J. Biol. Chem. 278 (2003) 32246–32250.
[10] A. Anishkin, S. Sukharev, Water dynamics and dewetting transitions in the small mechanosensitive channel mscs, Biophys. J. 86 (2004) 2883–2895.
[11] M. Sotomayor, K. Schulten, Molecular dynamics study of gating in the mechanosensitive channel of small conductance mscs, Biophys. J. 87 (2004) 3050–3065.
[12] B. Akitake, A. Anishkin, S. Sukharev, The "dashpot" mechanism of stretch-dependent gating in MscS, J. Gen. Physiol. 125 (2005) 143–154.
[13] J. Lu, M.E. Green, Simulation of water in a pore with charges: application to a gating mechanism for ion channels, Progr. Colloid Polym. Sci. 103 (1997) 121–129.
[14] M.E. Green, J. Lu, Simulation of water in a small pore: effect of electric field and density, J. Phys. Chem., B 101 (1997) 6512–6524.
[15] J. Lu, M.E. Green, Simulation of water in a small pore: effect of electric field and density II: immobilized molecules, J. Phys. Chem., B (1999) 2776–2780.
[16] O. Beckstein, P.C. Biggin, M.S.P. Sansom, A hydrophobic gating mechanism for nanopores, J. Phys. Chem. 105 (2001) 12902–12905.
[17] O. Beckstein, M.S.P. Sansom, Liquid–vapour oscillations of water in hydrophobic nanopores, Proc. Natl. Acad. Sci. U. S. A. 100 (2003) 7063–7068.
[18] O. Beckstein, M.S.P. Sansom, The influence of geometry, surface character and flexibility on the permeation of ions through biological pores, Phys. Biol. 1 (2004) 42–52.
[19] P.J. Corringer, N. LeNovere, J.P. Changuex, Nicotinic receptors at the amino acid level, Ann. Rev. Pharmacol. Toxicol. 40 (2000) 431–458.
[20] B. Corry, Theoretical conformation of the closed and open states of the acetylcholine receptor channel, Biochim. Biophys. Acta 1663 (2004) 2–5.
[21] B. Corry, An energy efficient gating mechanism in the acetylcholine receptor channel suggested by molecular and brownian dynamics, Biophys. J. 90 (2006) 799–810.
[22] A. Miyazawa, Y. Fujiyoshi, N. Unwin, Structure and gating mechanism of the acetylcholine receptor pore, Nature 423 (2003) 949–955.
[23] N. Unwin, Acetylcholine receptor imaged in the open state, Nature 373 (1995) 37–43.
[24] M.D. Edwards, Y. Li, S. Kim, S. Miller, W. Bartlett, S. Black, S. Dennison, I. Iscla, P. Blount, J.U. Bowie, I.R. Booth, Pivotal role of the glycine-rich TM3 helix in gating the MscS mechanosensitive channel, Nat. Struct. Mol. Biol. 12 (2005) 113–119.
[25] S. Miller, W. Bartlett, S. Chandrasekaran, S. Simpson, M. Edwards, I.R. Booth, Domain organization of the {MscS} mechanosensitive channel of *Escherichia coli*, EMBO J. 22 (2003) 36–46.
[26] O.S. Smart, J.M. Goodfellow, B.A. Wallace, The pore dimensions of gramicidin A, Biophys. J. 65 (1993) 2455–2460.
[27] B. Corry, T.W. Allen, S. Kuyucak, S.H. Chung, Mechanisms of permeation and selectivity in calcium channels, Biophys. J. 80 (2001) 195–214.
[28] M. Hoyles, S. Kuyucak, S.H. Chung, Energy barrier presented to ions by the vestibule of the biological membrane channel, Biophys. J. 70 (1996) 1628–1642.
[29] D.G. Levitt, Electrostatic calculations for an ion channel: I. energy and potential profiles and interactions between ions, Biophys. J. 22 (1978) 209–219.
[30] M. Hoyles, S. Kuyucak, S.H. Chung, Computer simulation of ion conductance in membrane channels, Phys. Rev. 58 (1998) 3654–3661.
[31] W.F van Gunsteren, H.J.C. Berendsen, Algorithms for brownian dynamics, Mol. Phys. 45 (1982) 637–647.
[32] W.F van Gunsteren, H.J.C. Berendsen, J.A. Rullmann, Stochastic dynamics for molecules with constraints: Brownian dynamics of *n*-alkanes, Mol. Phys. 44 (1981) 69–95.

[33] S.H. Chung, T.W. Allen, M. Hoyles, S. Kuyucak, Permeation of ions across the potassium channel: Brownian dynamics studies, Biophys. J. 77 (1999) 2517–2533.
[34] S.H. Chung, T.W. Allen, M. Hoyles, S. Kuyucak, Study of ionic currents across a model membrane channel using Brownian dynamics, Biophys. J. 75 (1998) 793–809.
[35] T.W. Allen, S. Kuyucak, S.H. Chung, Molecular dynamics estimates of ion diffusion in model hydrophobic and kcsa potassium channels, Biophys. Chem. 86 (2000) 1–14.
[36] S.I. Sukharev, B. Martinac, V.Y. Arshavsky, C. Kung, Two types of mechanosensitive channels in the *Escherichia coli* cell envelope: solubilization and functional reconstitution, Biophys. J. 65 (1993) 177–183.